Initial Implicit Changes in Adaptation as a Function of Different Perturbations

ZACCHARY NABAEE-TABRIZ

A THESIS SUBMITTED TO THE FACULTY OF GRADUATE STUDIES

IN PARTIAL FULFILLMENT OF THE REQUIREMENTS FOR THE DEGREE OF

MASTER OF ARTS

GRADUATE PROGRAM IN PSYCHOLOGY

YORK UNIVERSITY
TORONTO, ONTARIO

SEPTEMBER, 2025

Abstract

Implicit motor adaptation allows us to maintain accurate movements under changing conditions. This process, driven by sensory prediction errors (SPE), mismatches between predicted and observed sensory-motor outcomes, corrects motor commands unconsciously. This study examined the extent to which initial implicit adaptation is sensitive to error magnitude and whether it reflects the behaviour observed in prolonged exposure contexts. We employed a single-trial learning (STL) paradigm within a classical visuomotor adaptation task. Participants reached to dot and arc targets while experiencing single rotated-cursor trials (1°-90°), isolating trial-by-trial changes in motor outputs, along with a long-exposure block involving a 20° rotation to test STL predictability in prolonged contexts. Results suggest initial implicit adaptation follows a saturating response pattern with increasing error magnitude while model-derived predictions tracked reasonably with long-exposure performance. Our findings reveal key features of early implicit adaptation and highlight STL as a promising tool for examining implicit adaptation in varying contexts.

Acknowledgements

I would like to extend my most sincere thanks to Dr. Denise Henriques and Dr. Marius 't Hart for mentoring me over the last two years. Thanks to them, I developed a strong interest in the field of motor learning, a topic that was completely new to me upon first joining the lab. Their patience and dedication in helping me to overcome many of the challenges I encountered during my degree cannot be overstated. I am grateful for the support I've received from all of my lab mates in the SensoriMotor Control Lab, especially Raphael Gastrock and Parmin Rahimpoor-Marnani for their help over the course of this thesis, as well as the numerous volunteers who aided with data collection. I would like to also thank all of my BBCS friends with whom I've had the pleasure of studying alongside, specifically Soroush Ziaee, Felicia Tassone, Marium Alvi, Kiran Kaur Bumra, Emily Fewster, Ana Badal, Shaya Samet, Anthony Machula, and Yara Iskander. Our bi-weekly Thursday night outings provided me with laughs and good memories that I'll forever cherish. Finally, I'd like to thank my family for their continued love and support throughout this chapter of my life. I wouldn't be the person, or in the position that I am today without any single one of you.

Table of Contents

List of Figures

Introduction

Successful interaction with the environment relies on the motor system's ability to adapt to changes in feedback and novel movement demands. When executing movements, factors such as fatigue, injury, tool use, and changes to the environment can affect the accuracy and efficiency of the planned movement. To account for this, the human motor system possesses the innate ability to update motor commands with corrections that can ensure accurate and goal directed movement in spite of any ongoing changes to the body or environment (Bastian, 2008; Krakauer et al., 2019). Motor adaptation is one of the mechanisms that supports this ability to modify movements, occurring gradually through numerous recalibrations as the nervous system responds to changes in sensory feedback or physical constraints. When the consequences of planned movements are repeatedly altered, the brain consequently alters its motor outputs in order to minimize errors. A well-known paradigm used in motor adaptation research is visuomotor adaptation, where individuals make reaching movements while the visual feedback of their hand is manipulated. Here, a perturbation such as a rotated or fixed cursor creates a mismatch between the individual's expected and observed sensory movement outcome. Initially, individuals will experience fairly large performance errors where they miss their target. However with practice, they begin adjusting their movements to compensate for the perturbation and eventually re-establish accurate movement. This approach to studying sensorimotor recalibration provides an effective framework for probing the brain in how it identifies and accounts for movement errors.

In a typical visuomotor adaptation task, participants first practice reaching movements with aligned (veridical) cursor feedback, where the cursor accurately represents their hand position (Figure 1A). This phase allows participants to become familiar with the task and allows a baseline measurement of their reaching behavior. Once a perturbation is introduced, such as rotating the cursor's trajectory relative to the participant's hand movement (Figure 1B), participants initially experience errors, as the cursor no longer reaches the intended target. To compensate for the new change, the participants will make gradual adjustments to their movements in the opposite direction of the rotation over successive trials resulting in the cursor eventually realigning with the target. When visualized, participants will exhibit a particular learning curve where initial errors are large but decrease gradually as adjustments are made to

hand movements to account for the perturbation. As illustrated in Figure 2, this change in hand direction, to reduce cursor errors, follows an exponential learning curve, regardless of rotation size (as denoted by the different colours in Figure 2).

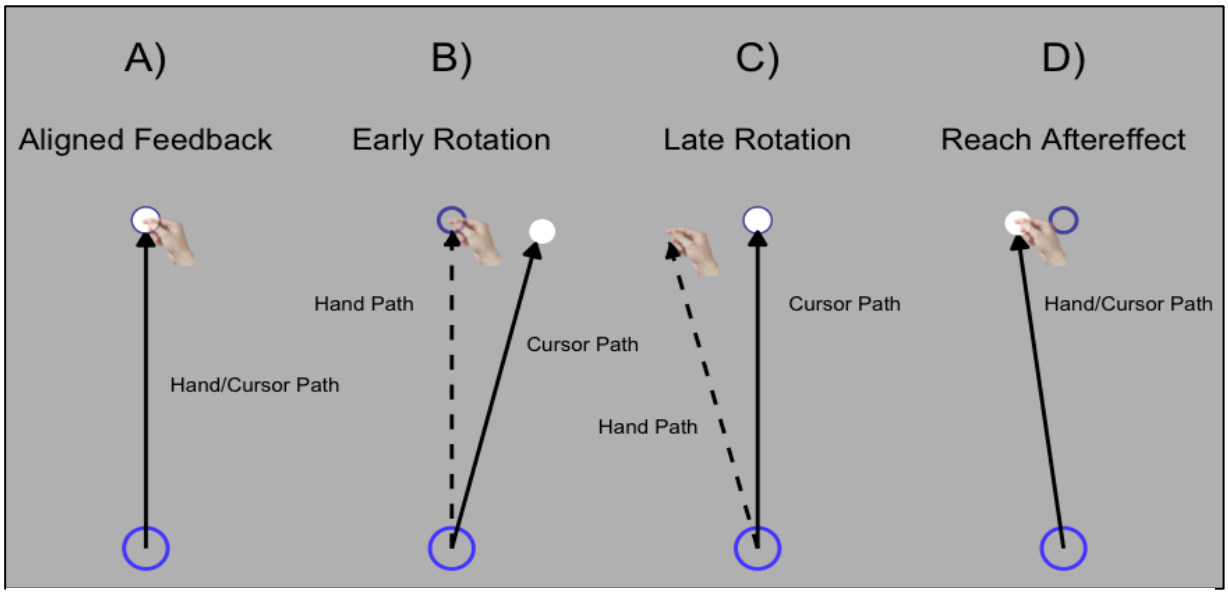

Figure 1. Example depicting performance in the early stages of visuomotor adaptation tasks. (A) Initially, participants will partake in trials with aligned (veridical) cursor feedback, where the cursor matches the position of their hand, to become familiarized with the task as well as for researchers to measure baseline behaviour. **(B)** When a rotation is initially applied to the cursor, participants will still reach toward the target but will notice that the cursor's trajectory is offset from that of their hand (rotated cursor feedback) and fails to reach the target. **(C)** With practice, participants learn to adapt to a given perturbation to the point where their reaches drive the cursor directly to the target. **(D)** Following a lengthy period of exposure, the perturbation is removed. For a short period of time, participants will continue to make involuntary corrective movements in their reaches as if the perturbation was still present, though these corrections will typically be smaller.

Beyond adapting their reaches to compensate for visuomotor rotations of varying magnitudes, this learning persists even after the perturbation is removed. As shown in Figure 2, when the cursor is made invisible and participants are instructed to reach toward the target using only their unseen hand (at movement bin 47), their movements continue to reflect the previously learned adjustments. These persistent hand deviations, known as aftereffects and also illustrated in Fig 1D, are systematic adjustments that remain even when participants reach for the same targets without the cursor or rotation. Even when explicitly instructed to move their unseen hand directly to the target, participants' reaches remain deviated in the direction previously used to counteract the rotation, though to a lesser extent than when moving with the rotated cursor.

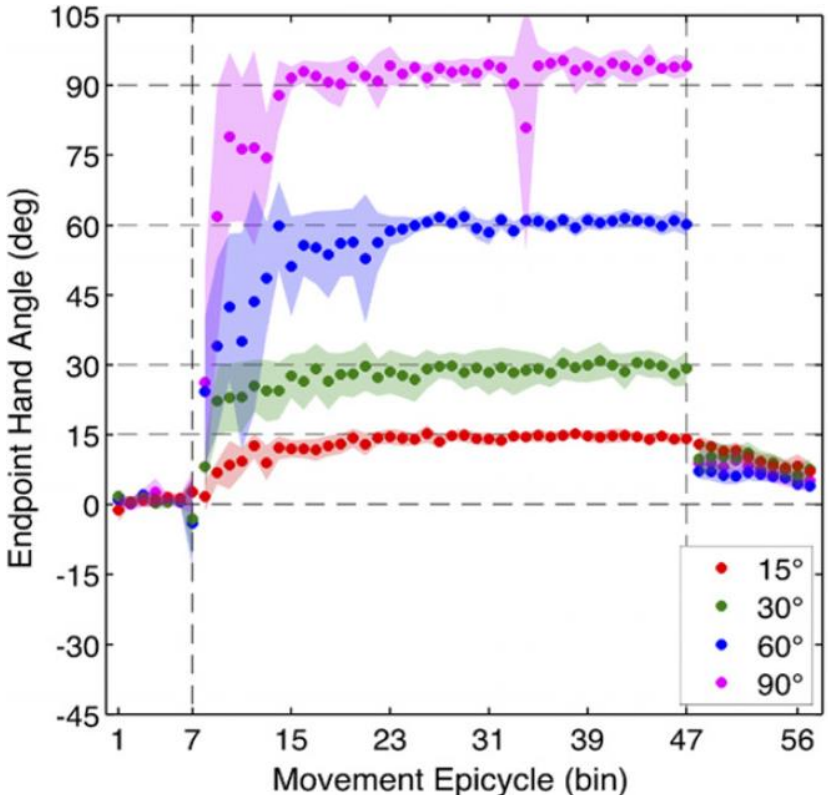

Figure 2. A plot of Experiment 3 from Bond & Taylor's (2015) study. Participants adapted to visuomotor rotations of 15° **(Red)**, 30° **(Green)**, 60° **(Blue)**, and 90°**(Purple).** Average direction of the unseen hand reach direction (relative to the target at the end of a reach) across movement cycles (bins of 8 trials). Rotations were introduced after 6 cycles (48 trials) and persisted for 40 bins (320 trials). Cursor feedback was then removed for the following 20 bins (160 trials) in order to measure residual learning. All participant groups successfully adapted to their respective rotations by the end of the rotation period.

Note: Learning time course of end-point hand angle. Reprinted from " Flexible explicit but rigid implicit learning in a visuomotor adaptation task", by K.M, Bond, 2015, *JNeurophysiol.* Copyright 2015 by the American Physiological Society.

These aftereffects are a distinctive feature of implicit adaptation, a branch of motor adaptation that recalibrates the motor system internally through sensory prediction errors (SPEs), mismatches between expected and observed sensory feedback (Krakauer et al., 2019) that force recalibrations of the internal forward model (Miall & Wolpert, 1996) at an unconscious level. This is supported by the fact that aftereffects are still evoked when participants are either made aware of the presence of a perturbation, or given instruction on how to counteract it, and are clearly instructed not to use any strategy once the cursor disappears (Gastrock et al., 2020; Mazzoni & Krakauer, 2006; Modchalingam et al., 2019; Neville & Cressman, 2018; Taylor &

Ivry, 2011). Therefore, aftereffects are inherently robust and automatic. When compared to explicit adaptation, which relies on conscious strategies (Taylor & Ivry, 2012), the extent of implicit adaptation appears to be limited from 10°-20° for perturbations between 15°-90° (Bond & Taylor, 2015; Kim et al., 2018; Modchalingam et al., 2019; Modchalingam et al., 2023; Morehead et al., 2017; Tsay et al., 2022; Zhang et al., 2024). The 'capped' nature of these aftereffects is again illustrated in Figure 2 for reach deviations for movement bins starting at bin 47. While reach aftereffects are a well-established measure of implicit adaptation, they are typically assessed only after extensive training (50-100, or sometimes more, trials), leaving open questions about how quickly these adaptative processes emerge. This study aims to examine a broad range of perturbation magnitudes to gain insight into the initial contributions of implicit adaptation.

More recently, a different paradigm has been developed that intends to capture unconscious changes in reach deviations by having participants move to targets with a fixed error direction (Al-Fawakhiri et al., 2023; Morehead et al., 2017; Kim et al., 2018, 2019; Zhang et al., 2024). Known as error-clamped training, this approach differs from classical visuomotor rotation paradigms in that all training-induced changes are assumed to engage only implicit processes. Here, the cursor follows a fixed deviation, unrelated to the hand movement, while participants are also instructed to move their unseen hand directly to the target and ignore the cursor, thus preventing explicit strategy use. However, despite being told to ignore the cursor, participants continue to unconsciously adjust their reaches as if compensating for the error. This allows researchers to isolate adaptation driven solely by unconscious and automatic mechanisms. However, the instruction to ignore the cursor makes this paradigm even less reflective of real-world adaptation when compared to traditional movement-contingent visuomotor tasks. Moreover, it is unclear whether the time course of adaptation in error-clamped paradigms mimics that of movement-contingent adaptation.

Recent findings suggest a promising approach for tracking the emergence and time course of implicit adaptation during classical movement-contingent tasks. Ruttle et al. were able to measure reach aftereffects after every 3-6 reach training trials (2016), as well as after every single reach training trial (2021, highlighting the ability of implicit aftereffects to emerge rapidly and saturate within as few as three training trials. In a preprint from our lab (D'Amario et al., 2024), reach aftereffects were also measured after each and every training trial, replicating the

finding of Ruttle et al., showing rapid emergence and saturation when using a perturbed cursor across different types of perturbations and rotation sizes (15°, 30°, 45°, and 60°). The initial change in these aftereffects was approximately 2–3° across different rotation magnitudes and experimental manipulations. This means that even after only a single training trial with a misaligned cursor, the subsequent reaches made without a cursor would deviate by a couple degrees. However, in this and other studies measuring the time course of implicit adaptation, we only assess this initial change or rate of learning once per participant. To better examine the initial implicit changes following training, the current experiment builds on these previous studies by implementing a single-trial learning (STL) paradigm. In this paradigm, reach aftereffects are measured after one individual learning trial, each followed by aligned washout trials. This approach allows for varying cursor perturbations across training trials, enabling repeated measurements of the initial implicit effect of training. In short, STL provides a more powerful assessment of early learning across many perturbation sizes, on a within-subject level.

The methodological advantages of single-trial learning have been used in a small set of more recent studies to explore key aspects of implicit motor adaptation that researchers were previously unable to probe. These include topics of research such as the asymmetrical relationship between error size and adaptive capacity (Hayashi et al., 2020; Marko et al., 2012; Vandevoorde & Orban-de-Xivry, 2019), the brain's differential processing of concurrent visual and proprioceptive error feedback (Hayashi et al. 2023), and the impact of task success manipulation on implicit adaptation (Al-Fawakhiri et al., 2023). Other studies have used STL to examine age-related differences in adaptation (Vandevoorde & Orban-de-Xivry, 2019), the effects of visual uncertainty on implicit learning (Tsay et al., 2021), as well as the ability to evoke implicit adaptation through sensory feedback alone without physical movement (Kim et al., 2022). To summarize, STL designs are very flexible in what they allow researchers to test. Given its methodological benefits, it would serve suitably for testing a wide variety of research questions, including that of the behaviour of initial implicit changes in adaptation. We use a STL to investigate the extent by which initial implicit changes vary with perturbation size, using a classical, movement-contingent paradigm. Research on the effects of perturbation size on the magnitude of implicit change is somewhat mixed. As mentioned earlier, several studies suggest that the extent of implicit changes does not vary much with perturbations larger than 20° in size, ranging between 10° and 20°, and that these implicit changes initially scale with small errors but

saturate for larger ones (Bond & Taylor, 2015; Kim er al., 2018; Morehead et al., 2017; Tsay et al., 2022). However, other studies suggest that as error size increases, implicit changes are attenuated and result in smaller adjustments being made to future movements (Tsay et al., 2021; Wei & Körding, 2009: Zhang et al., 2024). This is believed to occur as a result of the brain attributing larger errors to uncorrectable external factors due to a mechanism some researchers refer to as *error attribution* or *causal inference* (Körding et al., 2007; Wei & Körding, 2009). Therefore, larger errors will lead to a reduced unconscious response from the motor system. Nonetheless even with larger cursor perturbations, implicit changes do emerge, but it is not clear whether there is an effect of perturbation size on the initial implicit changes. D'Amario et al, only measured implicit adaptation for four rotation sizes (across different groups) and found that the initial change was larger for the group adapting to a 30° rotation (≈ 4°) compared to groups who trained with 15°, 45° and 60° rotations (≈ 2°). This was despite the fact that overall, the magnitude of aftereffects varied slightly, but positively with rotation size. Thus, the goal of this experiment is to rigorously measure the initial change of implicit processes across a large range of visuomotor rotations while also evaluating the STL's predictive power of initial implicit adaptation in prolonged exposure contexts. We hypothesize that initial implicit adaptation varies with perturbation size and that it will saturate as perturbation size increases given that there are more observed examples of a saturation effect in prolonged adaptation paradigms. We also hypothesize that STL possesses some level of predictive power of initial implicit adaptation in prolonged exposure contexts.

Methods

Participants

Participants (n = 129, M = 19.79 years, SD = 2.37, 92 Female, 36 Male, 1 Other/Prefer not to say, 0 excluded) from York University were recruited through the Undergraduate Research Participant Pool (URPP) and the Kinesiology Undergraduate Research Experience (KURE). Participants were then assigned to a version of the experiment with rotations of either ±1º, 5º, 10º, 15º, 20º, 25º, 30º, 35º, 40º, 45º (n = 30), ±1º, 5º, 10º, 15º, 20º, 25º, 30º, 40º, 50º, 60º (n = 43), or ±1º, 5º, 10º, 15º, 20º, 30º, 40º, 50º, 70º, 90º (n = 56). All participants provided informed consent during a pre-task questionnaire that collected demographic information. Participation in this experiment was completely voluntary, and all participants reported having normal or corrected-to normal vision.

Apparatus

As illustrated in Figure 3B, the experimental set-up consisted of a DELL E2009W monitor (44.30 cm length & 24.89 cm height) that was placed face down on a metal frame measuring 54 cm by 54 cm by 30 cm. Positioned 25 cm below the monitor was a mirror (50 cm by 35 cm) that faced upwards to reflect stimuli displayed on the monitor. Another 25 cm below the mirror was a Wacom Intuos Pro Large drawing tablet (44 cm by 27 cm). The aspect ratio of the tablet was mapped onto that of the monitor in order to maintain a 1:1 ratio with regard to movement. The position of the mirror projected the visual feedback to appear as if on the same horizontal plane as the participants' hand movements. The mirror also hid the view of the hand. A plastic stencil with a cone-shaped opening (8.5 cm radius) was attached to the tablet such that the downward tip coincided with the home position. This opening was slightly larger than the 8 cm distance of the targets, and its angle spanned a range of 160° as seen in Figure 3A & 4. The stencil constrained participants' movements to the designated workspace and also facilitated an easy return to the home position after each reaching movement.

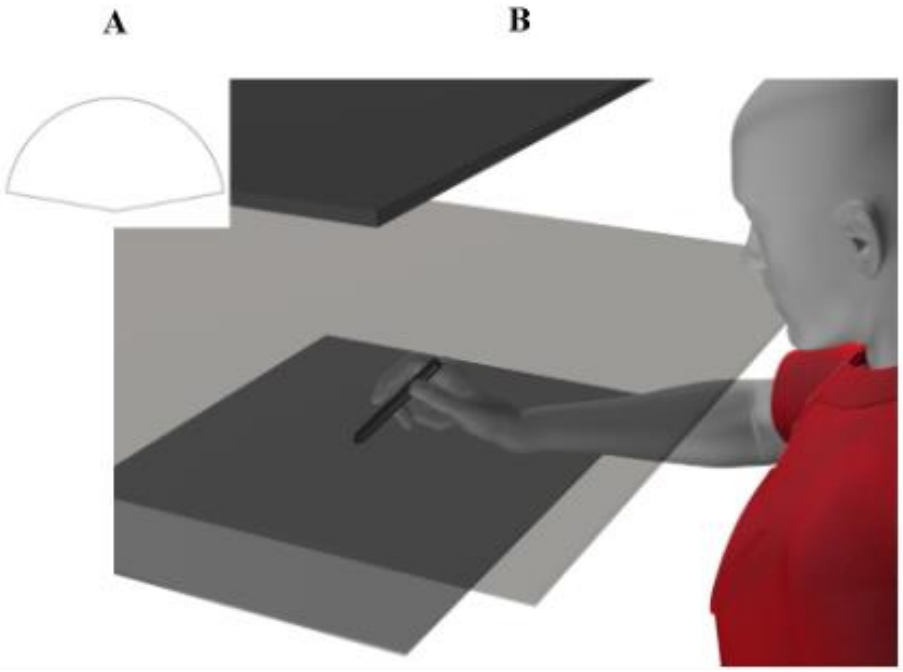

Figure 3. Experimental apparatus & stencil. Experimental apparatus included a DELL E2009W monitor on top, a Wacom Intuos Pro Large drawing tablet on the bottom, in addition to a mirror in the middle **(B).** The stylus is moved along the digitizing tablet, while the cursor's position is projected from the monitor above, and reflected off the mirror which occludes the participant's hand. Reaches were done within the cone-shaped stencil **(A)** situated on top of the digitizing tablet. (This figure was created alongside a selection of others by our lab for use in our various motor learning projects)

Experimental Procedure

Participants sat on height adjustable chair facing the experimental apparatus. Participants made outward reaches to visual targets using a stylus along the surface of the digitizing tablet. With their hand and arm beneath the mirror, they remain visually occluded. Reaches were initiated from a blue circular home position (5 mm radius), with a white circular cursor (3 mm radius) representing the stylus, toward a darker blue dot target that was also 3 mm radius at a radial distance of 8 cm from the home position. These small dot targets would randomly appear at either 60º, 75º, 90º, 105º, or 120º. For some trials this small dot target was replaced with a wide arc, spanning 120º from 30º- 150º relative to the home position, as seen in Figure 4. It should be noted that the use of different target types is meant to help answer a different research question being studied in a separate project, and the target type would alternate between each learning bout in the training phase of the experiment. However, the data obtained from both target types was used to help answer our research question.

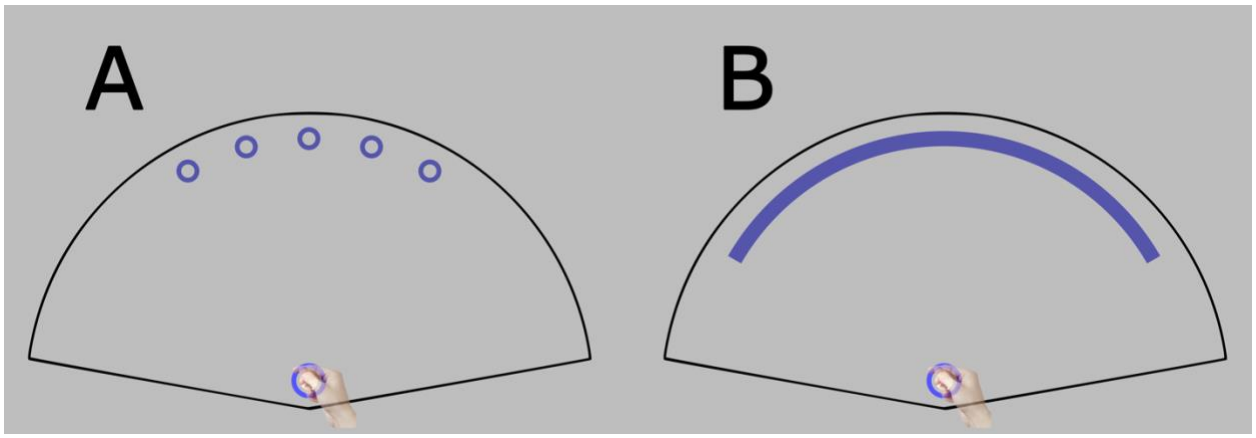

Figure 4. Target type variations. (A) Visual example of all possible dot target locations (60º, 75º, 90º, 105º, or 120º), followed by a visual example of the arc target **(B)**. Any part of the arc target may be reached. The 5 mm blue circle represents the home position, and the white circle represents the cursor. All targets are located 8 cm away from the home position. The stencil, which serves as the area where reaches may be done, surrounds both the dot and arc targets, as well as the home position. An added advantage of this cone-shaped stencil design is that it guides the stylus back to the home position following a reach, even when the cursor is not visible.

Participants were signaled to initiate the reach once a target appeared on the screen. Upon initiating a reach, the home position would disappear once the stylus travelled a radial distance of 0.5 cm away from it's centre, with the reach being considered completed once the stylus travelled a radial distance of 8 cm. At that point, the target and a static imprint of the cursor would remain for an additional 0.6 seconds, prompting participants to return the stylus to the home position for the next trial. During this time, the cursor would disappear, and the home position would reappear. Once participants returned the stylus to the home position, using the stencil to guide them (see Fig 4), and the cursor was held in place for 0.1 seconds, a new trial would begin. In each trial, once the cursor has been moved 2 or more radial cm away from the home position, the experiment samples the cursor's x/y positions relative to that of the home position [0,0] on the tablet while targets were specified in angular coordinates at a fixed radial distance of 8 cm.

Trial Types

Reaches were made with a cursor whose motion was either aligned (Fig. 1A) with their unseen hand or was rotated with respect to the hand (Fig. 1B). An aligned cursor, providing veridical feedback of the unseen hand to the participant, is used in the aligned-acquire, baseline, after-effects, and washout trials. The targets for aligned-cursor reaches were consistently small

dot targets as shown in Fig 4A. In contrast, rotated-training trials involved a visuomotor rotation of the cursor, with targets appearing as either a dot target located at 90º, or an arc target spanning 120º with its centre located at 90º.

Aligned-acquire trials were designed for participants to practice reaching while further reinforcing accurate reaches towards the targets, hence the cursor had to acquire, i.e. “overlap” with the target. They are found following mandatory 1-minute breaks (marked as vertical dashed lines). Baseline trials (Fig. 1A) were designed to assess participants’ baseline performance before introducing a visuomotor rotation to the cursor which occurred in the subsequent trial. Aftereffect trials (Fig. 1D) resemble baseline trials but assess persistent implicit learning following exposure to a rotated cursor during training (Fig. 1B). Changes in reach deviations were calculated between these, and baseline trials. Washout trials (Fig. 1A) were designed to help remove any residual learning left over from a previous rotation and appeared following aftereffects trials.

To complete baseline, rotation, after-effects, and washout trials, participants were required to move the cursor such that there is a radial distance of 8 cm between the cursor and the home position, whereas aligned-acquire trials required the centre of the cursor to fall within the target, emphasizing accuracy. Moreover, auditory feedback contingent on reaction time, measured from the moment the target appeared, and movement time, measured from the onset to the end of a reach, was presented at the end of all trials. If a participant's reaction and movement times fell within 0.15s – 10.0s and 0.2s – 0.4s respectively, they were provided with positive auditory feedback. The reaction time range was chosen to allow for participants to see the target and plan their reach which could be reflected in their initial movement direction. By contrast, the movement time range was chosen to motivate participants in following a constant pace of fast reaches.

Single-Trial Learning Bouts

To capture early implicit learning, we used Single-trial learning (STL) bouts to repeatedly test the effects of multiple single-rotation exposures. These bouts are essentially small learning blocks that could consist of 4, 5, or 6 trials. Within each bout, all trials except one featured zero rotation. The sequence of trials in each bout included: a baseline trial (first trial, Fig. 1A), a rotation-training trial with a misaligned hand-cursor (second trial, Fig. 1B), and an after-effect trial (third trial, Fig. 1D). These were followed by 1, 2 or 3 washout trials (Fig. 1A). The number

of washout trials between STL bouts was pseudorandomized to reduce the likelihood of participants predicting when a rotation may occur. Additionally, the size of the visuomotor rotation was pseudorandomized across STL bouts, with three groups exposed to different ranges of rotations. The range of rotations shared amongst all groups included ±1º, 5º, 10º, 15º, 20º, 30º, and 40º. However, the 45º-max group, which had a smaller range of rotations, additionally included ± 25º, 35º and 45º, the 60º-max group, with a larger range, included ± 25º, 50º, and 60º, while the 90º-max group also included ± 50º, 70º and 90º. This way, each group would be tested on a range of 10 rotation magnitudes. Each rotation magnitude was presented five times across both directions (CW and CCW) for both dot and arc target types. Initial changes in implicit adaptation were calculated within STL bouts by comparing changes in reach deviation between baseline and after-effects trials for a given STL bout, though this is further explained in our section on data preprocessing.

Experimental Phases

As shown in the perturbation schedule in Figure 5, the study was divided into several phases (marked by vertical dashed lines), with mandatory breaks of at least one minute at the end of each phase. Additionally, within the STL phase, breaks were scheduled every ~240 trials. This schedule illustrates the pseudo random rotations applied to the group experiencing a maximum ±60º cursor rotations. As can be seen in this example schedule, the majority of trials in the schedule have a 0° rotation, as they represent trials with aligned (unperturbed) cursor feedback, and thus look flat in the schedule. The vertical lines indicate when the single rotation was introduced, specifying its magnitude, direction, and trial number. The color of each line further distinguishes whether the target was a dot (blue) or an arc (orange). The exact magnitude and direction of the perturbation, along with the number of trials (to a lesser extent), were randomized across participants in both the 45° and 60° max groups. The number of subsequent washout trials also varied, as described below, and thus the “timing” or trial number of the rotation trials differed slightly across randomized schedules.

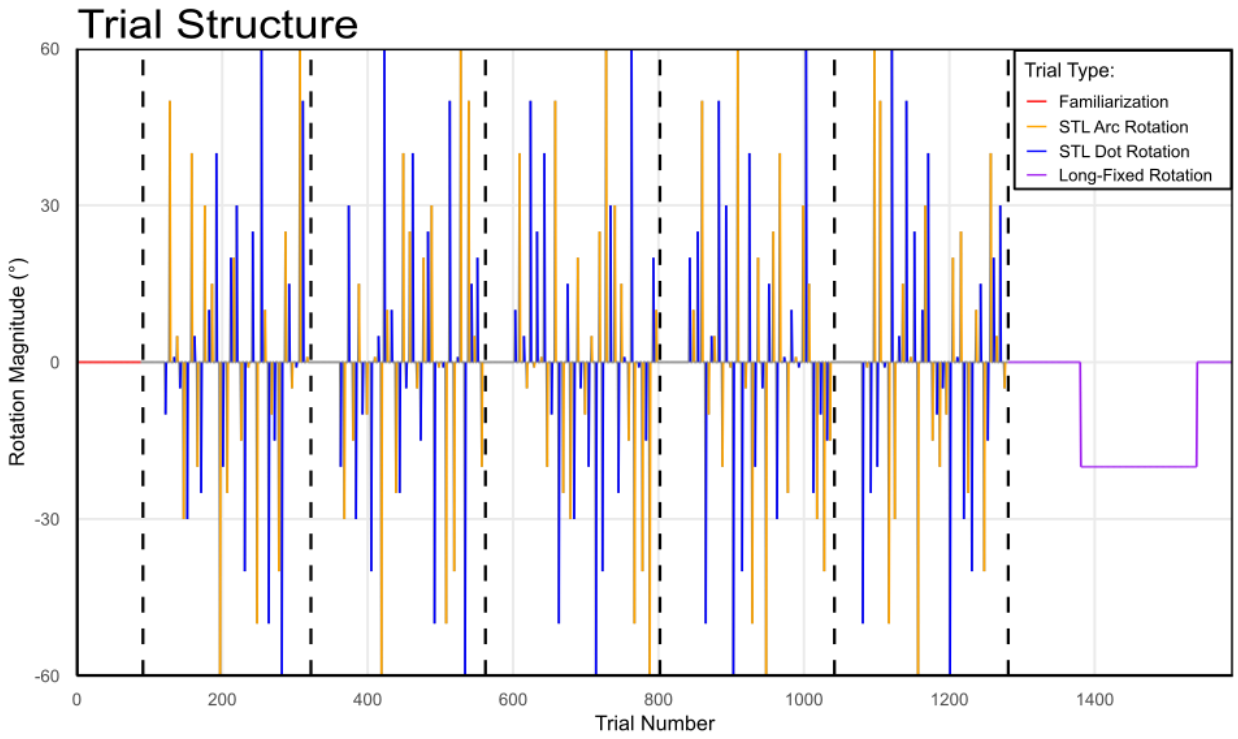

Figure 5. Example of the trial structure from the three main experimental phases. The Familiarization phase **(trials 0 – 80)**, consists of 40 familiarization trials with the circular target, followed another 40 trials with the arc target. The STL phase **(trials 81 – 1281)**, consists of 1200 trials. STL bouts are made up of 1 baseline, 1 rotation, 1 aftereffects, and 1 – 3 washout trials. The rotation values are pseudorandomized from bout to bout. The Long-Fixed Rotation Phase **(trials 1282 – 1591)** consists of 310 trials: 40 aligned-acquire trials, 60 baseline trials, 160 rotation trials with a fixed rotation of -20°, followed by 25 after-effects and 25 washout trials. Black vertically dashed lines represent mandatory 1-minute breaks. The first 40 trials following each break consisted of 10 aligned-acquire trials, followed by 30 baseline trials.

Familiarization

The experiment began with a familiarization phase to allow participants to get used to the setup and task requirements. It consisted of 80 familiarization trials, where participants were made to reach towards the dot target for the first 40 trials, and the arc target for the latter 40 trials. Trial completion for this phase only required that the stylus travel 8 radial cm away from the home position.

Single-Trial Learning

Following familiarization, participants were introduced to the single-trial learning (STL) phase of the experiment. Before beginning, they were reminded to make straight and fast reaches

towards the targets. Additionally, they were notified that for some trials, the cursors may not behave as expected but to still try and focus on reaching towards the targets. The STL phase lasted approximately 1200 trials, with slight variation due to the pseudo-randomization of washout trials. However, while the rotation magnitude between STL bouts was pseudo-randomized, the target type presented in the rotation trial of each bout would alternate between the dot and arc target.

Long Fixed Rotation

The latter half of the experiment involves a long-fixed rotation (LFR). Consisting of 310 trials, the LFR phase began with 40 aligned-acquire trials, followed by 60 baseline trials, 160 rotation trials, 25 after-effects trials, and 25 washout trials. For the rotation trials, all participants experienced a predetermined fixed rotation value of -20º. This was chosen to reflect the commonly observed maximum implicit adaptation between 10° and 20° (Morehead et al., 2017; Kim et al., 2018; Modchalingam et al., 2023) without also evoking other contributions to adaptation. The data obtained from this phase was used to help us understand whether STL performance could generalize to performance in prolonged exposure contexts.

Data Analysis

Preprocessing

As mentioned in the apparatus subsection, the cursor position is sampled in each trial once it has been moved 2 or more radial cm away from the home position. From this, the reach direction was calculated as the angle of the movement vector from the home position to the sampled trajectory point, and the angular reach deviation was calculated as the difference between the reach direction and the ideal target vector relative to the home position in degrees. This 2-cm mark is meant to capture the direction of the early, planned, or "ballistic" component of the outward movement, as opposed to any feedback-dependent corrections. To assess initial changes in implicit adaptation, we measured changes in angular reach deviations between baseline and aftereffect trials within each STL bout as part of the data collection. For clarity, we refer to this change, representing the difference in reach angle before and after each single rotated trial, as an aftereffect. Since it reflects the immediate trials following the rotated training trial, it captures the initial implicit changes associated with reaching under the rotated target condition. Next, we removed any trials (n = 29) with aftereffects that deviated more than -60º and 60º as outliers. We do not analyze reach training within the STL, so this cut-off for the initial aftereffect should be reasonable, given that most reach aftereffects following longer training bouts typically do not exceed 20º.

Preliminary Analyses

To verify that our task successfully elicited implicit learning, we first checked whether reliable aftereffects were present. To do this, reach deviation data was collapsed across rotation sign and then normalized, ensuring all errors fell on a positive scale. For each rotation size and target type, we computed the median aftereffect within each participant and then averaged those medians across participants. We used a bootstrap procedure to generate 95% confidence intervals around these group means. If the confidence intervals excluded zero, we interpreted this as evidence of a reliable aftereffect, indicating that the motor system had adjusted in response to the perturbation.

Next, we examined whether our observed aftereffects varied depending on rotation size by conducting repeated-measures ANOVAs within each rotation group. This analysis tested for a

main effect of rotation size, target type (dot vs. arc), or interaction between the two, on observed aftereffects. However, our main interest was the main effect of rotation size, which would indicate that initial implicit adaptation differs across rotation sizes and thus justify subsequent modeling of its behaviour.

Model Fitting

To evaluate how initial adaptation depends on perturbation size, we fitted each participant's aftereffect data to two competing models that reflect previously observed behaviours of attenuation and saturation with increasing error size: the *Attenuation* and *Capped Fixed-Rate* models. An example of each model's expected behaviour can be seen in Figure 6.

Attenuation Model

The attenuation model operates on the assumption that as participants encounter increasingly large errors, they are less likely to be attribute to themselves, leading to an eventual decrease in initial implicit adaptation. Our model uses a gaussian density function to convey this idea and can be expressed as:

$$P(x) = x \cdot s \cdot \mathcal{N}(x, w)$$

Here, $x(p)$ represents a predicted reach deviation for a rotation of size p, s serves as a scaling factor accounting for the fraction of the error that is corrected when error attribution is deemed as internal, $\mathcal{N}$ represents a normalized gaussian probability density function, and w, representing error sensitivity, serves as the variance:

$$\mathcal{N}(x, w) = e^{-\frac{x^2}{2w^2}}$$

By setting a mean value of 0 and normalizing the function to equal 1 at this mean, we can simplify the function so that predicted reach deviations equal the fractional correction when rotation values are close to 0. In short, this model is meant to reflect the idea that initial implicit adaptation decreases for very large error sizes.

Capped Fixed-Rate Model

The capped fixed-rate model operates on the assumption that beyond a certain rotation size, initial implicit adaptation is capped and stays constant regardless of further increases to the

rotation size. By using a cap level beyond which implicit adaptation cannot increase, and a fractional correction rate displaying the amount of error that can be corrected for on a given trial, we can express the model as such:

$$P(x) = min(c, r \cdot x)$$

Here, $x(p)$ still represents the predicted reach deviation, c represents the cap level, r represents the fractional correction rate, and p represents the rotation size.

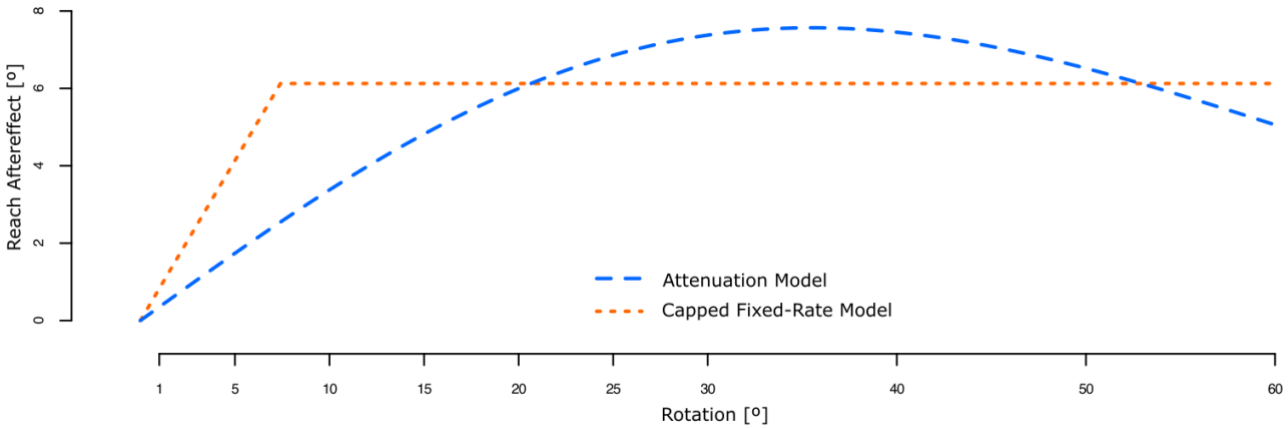

Figure 6. Example visualizing expected behaviour of reach aftereffects across a range of perturbations (1 - 60°). In the Attenuation model **(Blue)**, implicit adaptation increases for smaller errors but decreases for larger errors. In the Capped Fixed-Rate Model **(Orange)**, adaptation initially scales linearly with smaller errors but saturates (or caps out) as errors get larger.

To obtain capped *(c, r)* and attenuated *(s, w)* parameter sets for each participant, we used a grid search followed by bounded optimization which allowed us to sample the parameter space while minimizing the risk of local minima. For each model and participant, the 10 parameter sets yielding the lowest mean squared error (MSE) between model predictions and observed aftereffects were then optimized to obtain a single parameter set with an even lower MSE, which was then chosen for fitting. Model fits were first compared at the group level through MSE and corrected Akaike Information Criterion (AICc) values, providing us with insight as to each models' relative goodness of fit and complexity. Comparisons were then made at the individual level by conducting paired-sample *t*-tests on the MSE values of all participants.

Prolonged Exposure Predictability from Single Trial Learning

To examine whether STL-based model predictions could generalize to performance seen in prolonged sensorimotor adaptation, we compared each participant's predicted adaptation to their observed behaviour during the long-fixed rotation phase, a 310-trial long exposure block containing 160 consecutive rotation trials involving a -20° rotation. For each participant, we estimated adaptation following the first rotated trial by fitting an exponential decay function to their full learning curve across all 160 / 310 trials, and taking the value following the first rotated trial. Similarly, we fitted both the attenuated model and the capped fixed-rate model to each participant's STL data with dot targets only, and took the fitted value for a 20° rotation. If these are comparable indices of learning then, they should be roughly equal. Plotting one over the other, the points should fall close to a unity line passing through the origin with a slope = 1. To test this, we then conducted linear regressions, with the intercept set to 0, of our exponential predictions onto the STL-based model predictions, separately for the capped fixed-rate and attenuation models within each rotation group. In these regressions, the slope of the fit reflects how closely STL predicts adaptation in the long-fixed rotation phase: a slope of 1 would indicate perfect prediction, whereas a slope < 1 would suggest overestimation and a slope > 1 would suggest underestimation. Model performance in this context was compared using AICc values and R^2 from the regression fits.

Since our results indicated overestimation by the STL model fits, we also wanted to test the alternative; underestimation of initial learning by the exponential function fit to the long exposure data. To test this, we directly compared each participant's exponential fit estimate to their actual reach behaviour following the first rotated trial of the long-fixed rotation phase. Paired-sample *t*-tests were used to evaluate whether the model-based prediction and the observed reach deviation differed significantly. This analysis helped confirm whether the observed overprediction from STL models was due to genuine differences in adaptation behaviour or artifacts introduced by curve fitting.

Results

To examine the effect of perturbation size on initial implicit adaptation, 129 participants completed a Single Trial Learning (STL) paradigm involving pseudorandomized cursor rotations trials that reached a maximum size of either 45º (n = 30), 60º (n = 43), or 90º (n = 56). Implicit learning was quantified through trial-by-trial changes in angular reach deviations between baseline and aftereffects trials within each STL bout.

Effect of Perturbation Size on Implicit Motor Adaptation

We aimed to verify the presence of significant aftereffects in our data, as seen in Figure 7 which illustrates the relationship between perturbation size and initial implicit reach aftereffects across the 45°-max, 60°-max, and 90°-max rotation groups. The blue curves in this figure show the initial aftereffects following training with a small circular target, while the orange curves represent aftereffects following training with a wide arc target. The overall pattern as a function of rotation was largely similar across the two conditions (no significant interaction of target type and rotation size) for each of the three groups and so aftereffects for both targets were used for subsequent analyses.

Apart from 1° rotation trials with arc targets, we observed reach aftereffects across all rotation sizes in all three rotation groups, as indicated by their confidence intervals lying above zero (Fig. 7A, 7B, 7C). Additionally, reach aftereffects appeared to scale with smaller rotations of 1°- 15°, before settling around 6° for larger rotations of 15º- 90°. We then aimed to determine whether the implicit aftereffects we observed in Figure 7 were statistically significant, meaning the aftereffects were different for different rotation sizes. Repeated-measures ANOVAs showed a main effect of rotation size in the 45°-max group ($F(5.80, 168.27) = 13.03$, $p < .001$, $\eta^2g = .147$), the 60°-max group ($F(6.84, 287.36) = 19.95$, $p < .001$, $\eta^2g = .149$), and the 90°-max group ($F(7.33, 403.41) = 19.27$, $p < .001$, $\eta^2g = .127$). Together, the presence of reach aftereffects as well as the consistent main effect of perturbation size across all groups demonstrates that implicit motor responses are sensitive to the size of the experienced error, at least up to approximately 15°, beyond which adaptation may saturate.

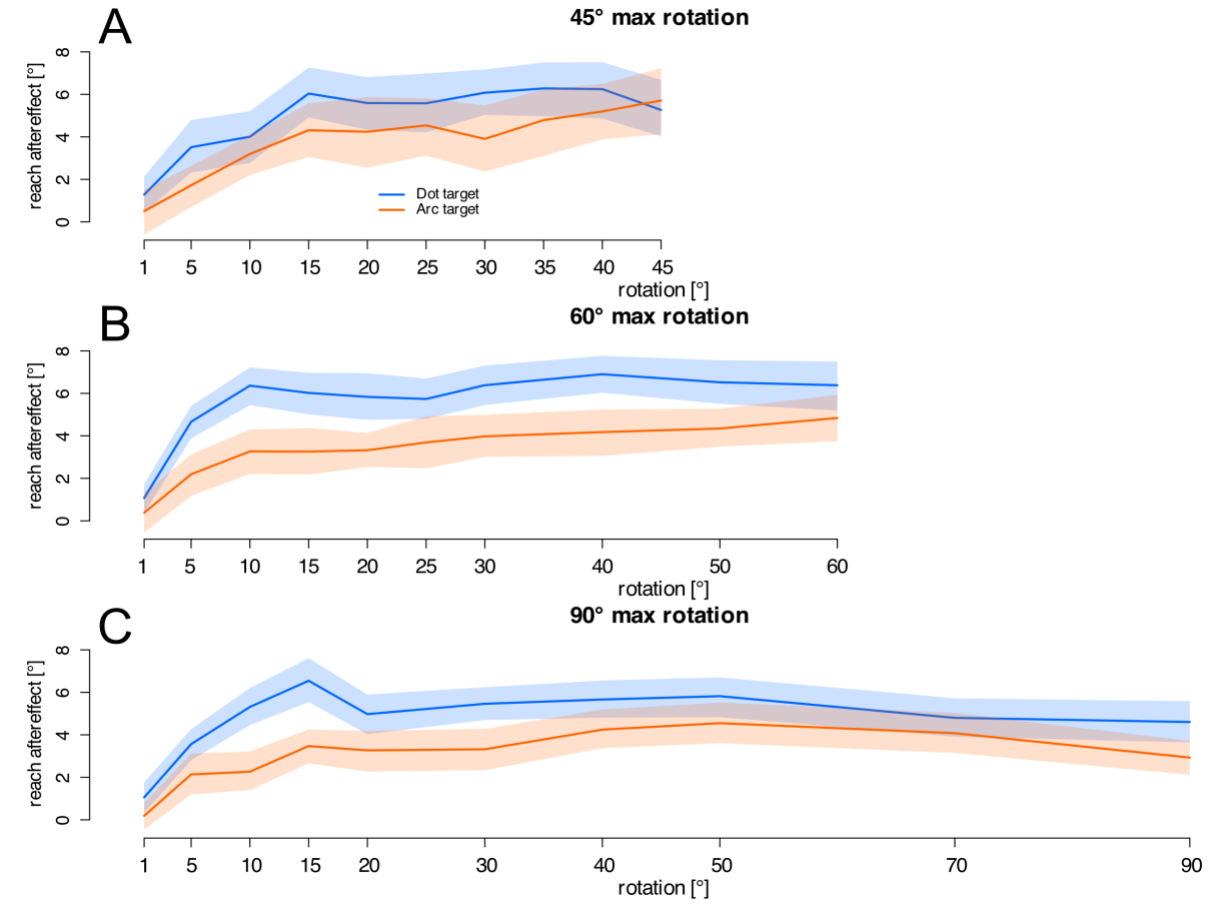

Figure 7. Initial change across rotation groups. Initial changes in implicit reach aftereffects measured across the respective ranges of rotations in the 45° **(A)**, 60° **(B)**, and 90° **(C)**, maximum rotation groups. Blue line data represents average reach aftereffects in dot target trials, while orange line data represents that of the arc target trials. Shaded regions represent bootstrapped 95% confidence intervals of mean initial change for each target type.

Effect of Rotation Size on Implicit Adaptation: Capped Fixed-Rate vs. Attenuation Model

To characterize how initial implicit motor adaptation changes with perturbation size, we fitted our attenuation and capped fixed-rate models to STL reach data from individual participants across rotation groups, as well as target type. As shown in Figure 8 (Panels A–C), both models track the group-level data reasonably well. However, the capped fixed-rate model more accurately reflects the pattern of adaptation observed in the data given that adaptation appears to initially increase with rotation before levelling off around 5–6°, especially in the dot target condition. In contrast, the attenuation model predicts that adaptation should decrease at larger rotations, but this downward trend doesn't appear to be supported by the plots.

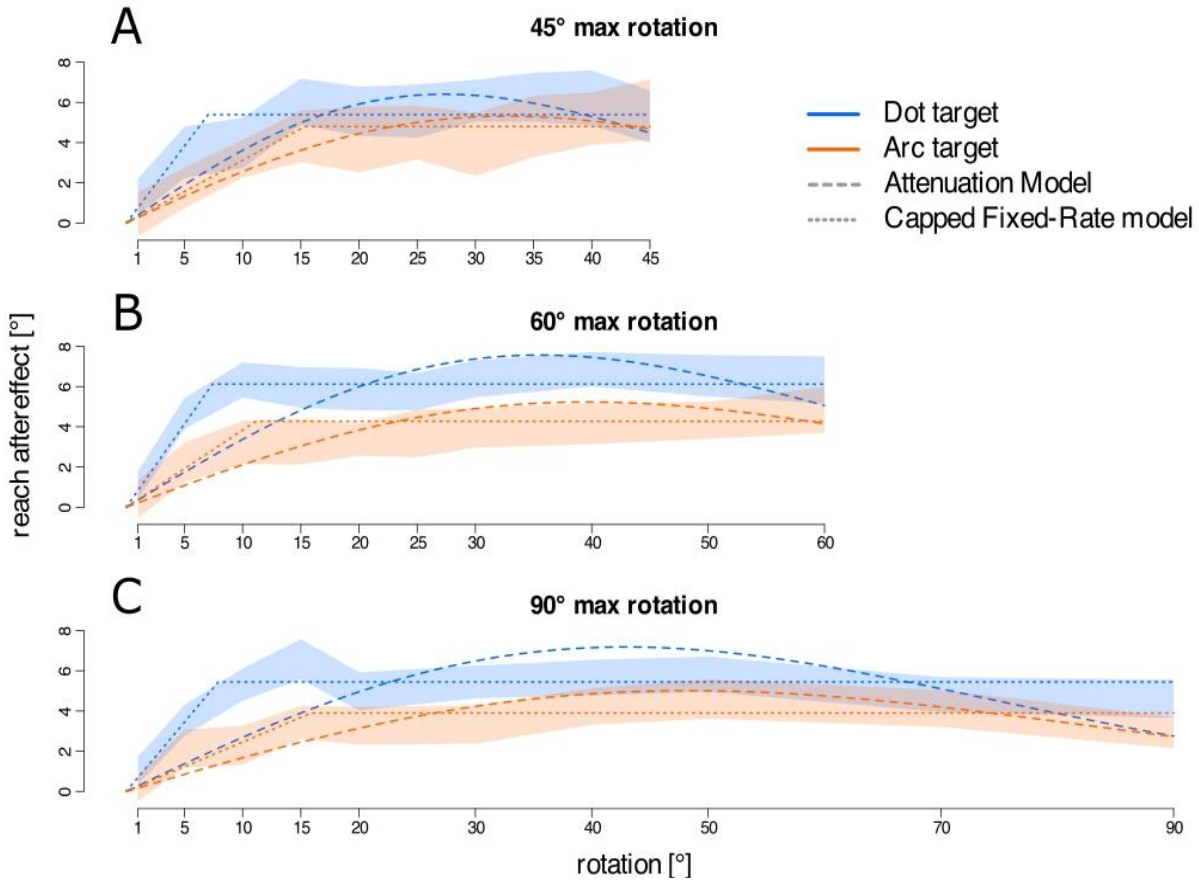

Figure 8. Fitted model predictions. Fitted predictions of the capped fixed-rate (dotted lines) and attenuation (dashed lines) models for the 45° group **(A)**, the 60° group **(B)**, and the 90° group **(C)**. Plotted separately for dot (blue) and arc (orange) targets. Shaded regions indicate the bootstrapped 95% confidence interval of the group means.

In an effort to determine whether this difference in fit was consistent across participants, we conducted a paired-samples t-test comparing each participant's MSE for the two models, as shown in Figure 9. Results revealed the capped fixed-rate model produced lower MSEs than the attenuation model, ($t(257) = –9.12$, $p < .001$, 95% CI [–2.10, –1.36]), with a mean difference of –1.73, meaning the capped fixed-rate model's predictions were on average, 1.73° closer to participants' actual reach behaviour. Our capped-fixed rate model also returned a lower corrected Akaike Information Criterion (AICc = 54.68) than the attenuation model (AICc = 54.92), indicating a slight advantage in fit quality. Relative log-likelihoods computed from these AICc's show a better fit for the capped fixed-rate model, this does not however, reach significance ($p = 0.89$). We also plotted each participant's model MSEs, as seen in Figure 9, where most points fall close to the unity line, and only some show a clearly better fit for the capped fixed-rate model, i.e. a larger prediction error for the attenuation model. In sum, while the evidence in our data set

is not very strong, it does seem that the capped fixed-rate model predicts the data better. Moreover, our findings suggest that initial implicit motor adaptation increases with rotation size up to a fixed limit, beyond which further increases in error do not lead to any differences in initial implicit adaptation.

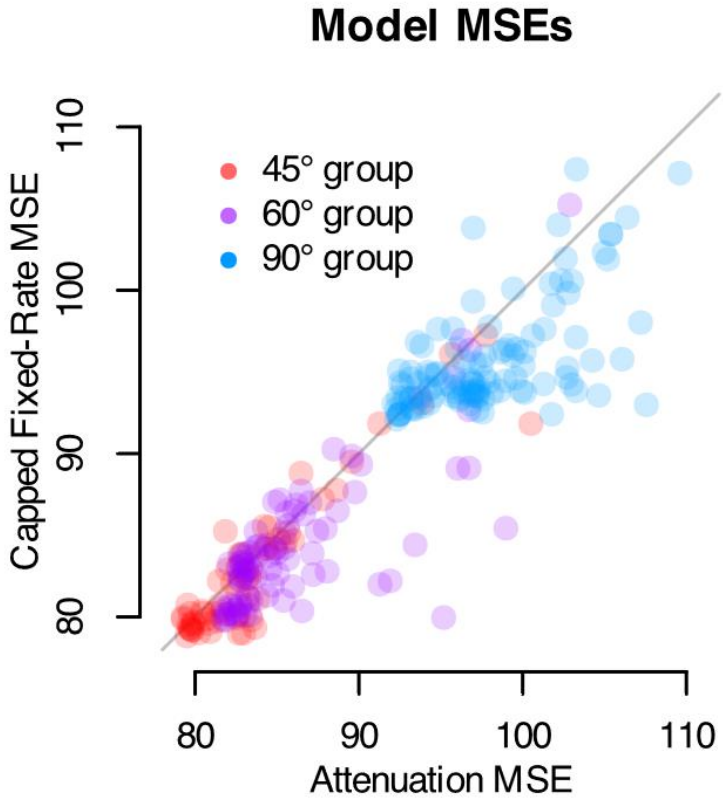

Figure 9. **Model fit comparison across participants.** Each point represents a single participant's mean squared error (MSE) for the capped fixed-rate model (y-axis) and the attenuation model (x-axis), computed from single-trial learning fits between the 45° **(Red),** 60° **(Purple)**, and 90° **(Blue)**, rotation groups. The diagonal line indicates the unity line (i.e., equal model fits). Points located further away from the unity line indicated a poorer fit with respect to the model they are closer to.

Predicting Implicit Adaptation in Prolonged Exposure Training from Single Trial Learning

To evaluate whether single-trial learning generalizes to prolonged sensorimotor adaptation, we tested how well STL-based model predictions aligned with adaptation behavior during our long fixed-rotation phase which included a 160-trial long exposure block under a 20° visuomotor rotation. For each participant, we estimated initial adaptation following a single rotated trial by fitting an exponential decay function to their learning curve and taking the value

of the function after the first rotated trial. This was done for each rotation group, using only dot target trial data to compute our predictions. As shown in the left column of Figure 10 (panels A-C), participants in all three rotation groups successfully adapted to the rotation. If the two measures perfectly align, they should fall on the identity line, i.e. the slope is 1 and the intercept is 0. Here we forced the intercept to be 0 and assessed how well STL predictions aligns with long exposure adaptation by looking at the fitted slopes, R^2, and p -values for each model and group.

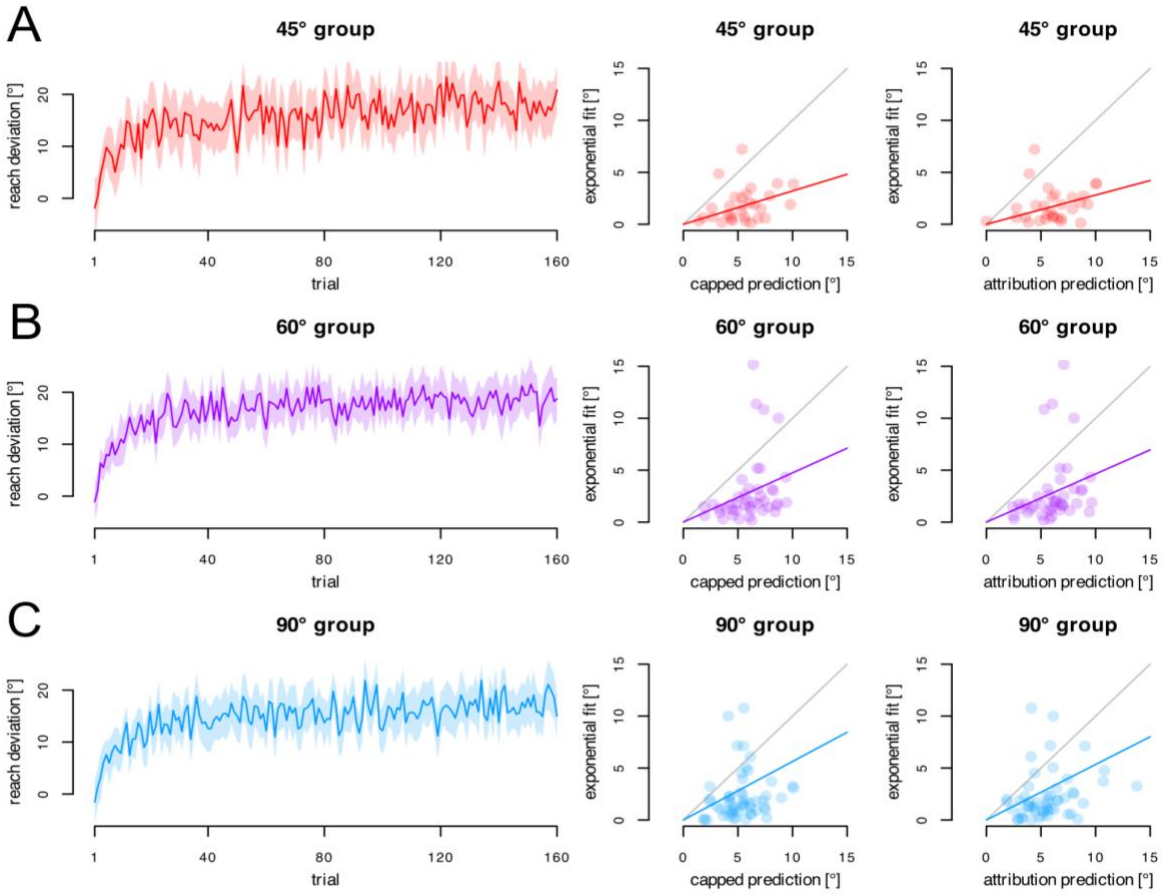

Figure 10. Predicted initial adaptation. Predictions of initial implicit adaptation in the long-fixed rotation phase based on single-trial learning across the across the 45° **(A)**, 60° **(B)**, and 90° **(C)** rotation groups. Left panels depict average reach deviations over 200 trials in the long exposure block, with shaded regions representing 95% CI and superimposed exponential fits. Middle and right panels show the predicted reach deviations from the capped fixed-rate and attenuation models, respectively, plotted against corresponding exponential fit estimates.

Visually, predictions from both the capped fixed-rate and attenuation models appeared to be related with these early adaptation estimates. For the 45°-max group, the capped fixed-rate model yielded a slope = 0.32, ($t(29) = 6.50$, $p < .001$, $R^2 = .593$, AIC = 115.24); while the

attenuation model produced a slope = 0.28, ($t(29) = 6.08$, $p < .001$, $R^2 = .560$, AIC = 117.53). In the 60°-max group, the capped fixed-rate model showed a slope = 0.47, ($t(42) = 6.46$, $p < .001$, $R^2 = .498$, AIC = 221.05), and the attenuation model had a slope = 0.46, ($t(42) = 6.21$, $p < .001$, $R^2 = .479$, AIC = 222.70)). In the 90°-max group, the capped fixed-rate model yielded a slope = 0.56, ($t(55) = 5.91$, $p < .001$, $R^2 = .388$, AIC = 318.49), and the attenuation model yielded a slope = 0.53, ($t(55) = 6.13$, $p < .001$, $R^2 = .406$, AIC = 316.81). The positive nature of these slopes suggests that STL has relevance in predicting prolonged learning outcomes. That is, there was a strong linear relationship between all STL-based predictions for the 20° rotation, and the exponential error function's value after 1 trial with 20° rotated feedback (all p<.001). The slopes also indicate slightly better predictions by the capped fixed-rate model. However, all of the slopes fell well below 1.0, hinting at an overestimation of the actual amount of adaptation observed in the long fixed-rotation phase. These overestimations are also visible in the middle and right columns of Figure 10 (panels A- C) where much of the predictions fall below the identity line.

In contrast, it could be that the exponential fit may have actually underestimated the initial learning. To assess this, we compared the exponential fit's prediction of adaptation after one rotated trial to the actual reach deviation on that trial using paired *t*-tests. As shown in Figure 11, observed reach data varied much more than the exponential functions (which are indeed meant to reduce noise in the estimates), at times showing movement in the wrong direction, while exponential fit predictions were visibly higher, hinting at possible overestimation, but more stable. Paired t-tests revealed no significant difference between exponential predictions and observed reaches in any group: 45°-max group: $t(29) = 0.84$, $p = .408$, mean difference = 1.54°, 95% CI [–2.21, 5.29]; 60°-max group: $t(42) = 1.04$, $p = .302$, mean difference = 1.70°, 95% CI [–1.59, 4.99]; 90°-max group: $t(55) = 1.15$, $p = .257$, mean difference = 1.82°, 95% CI [–1.36, 5.01]. These results suggest that the exponential function does not systematically underestimate early adaptation, leading back to the original assumption that the STL predictions may overestimate initial early adaptation.

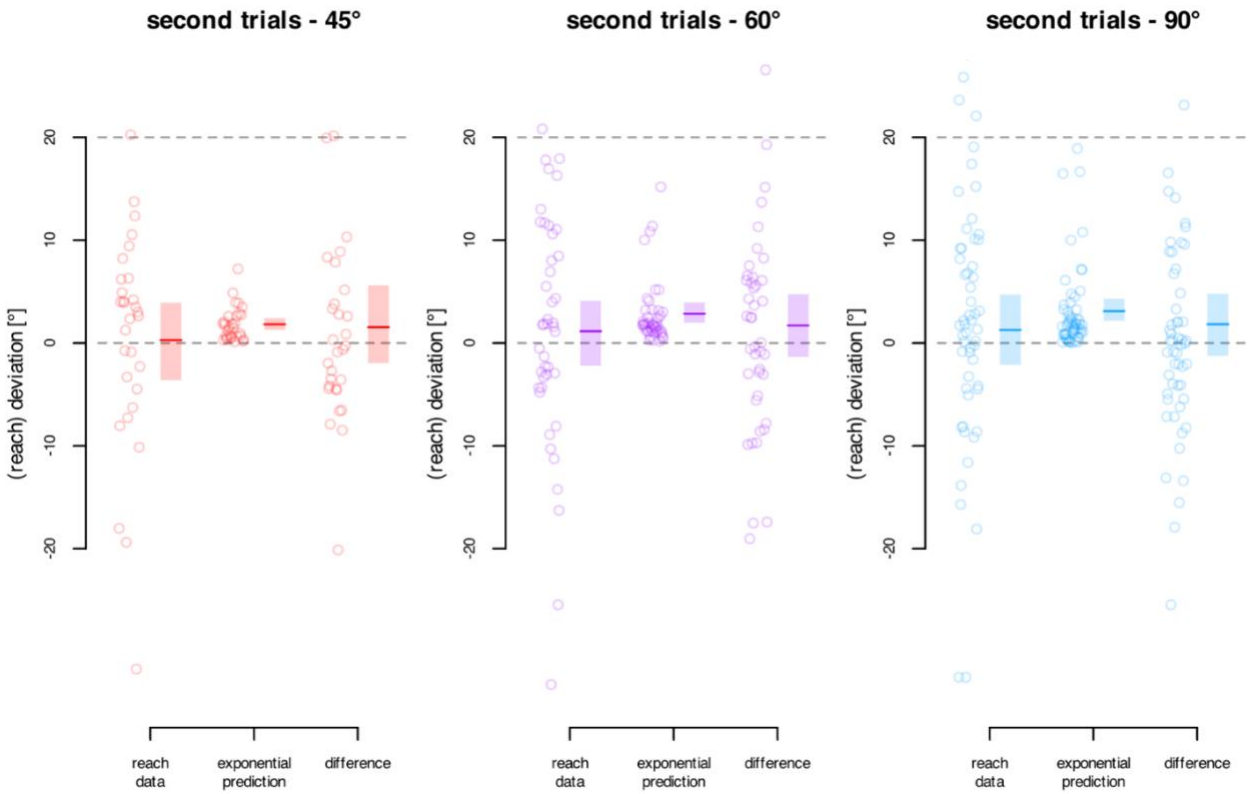

Figure 11. Comparison of exponential model predictions and observed reach behaviour. Exponential model predictions of initial implicit adaptation after the first rotated trial in the 45° **(Red)**, 60° **(Purple)**, and 90° **(Blue)** rotation groups were compared against observed reach behaviour. Each panel plots the fitted estimate of initial adaptation derived from the exponential decay function against the actual reach deviation recorded after the first trial of the long-fixed rotation phase. Dots represent individual participants, coloured horizontal lines represent group mean, and shaded vertical bars represent 95% CI.

Overall, our findings demonstrate that initial contributions in implicit adaptation are systematically influenced by perturbation size. Training using single trial-learning (STL) produced significant implicit reach aftereffects across rotation size. Notably, exposure to a 1° rotation with dot targets was able to evoke significant motor responses, though not when using arc targets. As rotation size increased, initial implicit aftereffects scaled accordingly before saturating around 6° for rotations of, or larger than 15º. This pattern in reach behaviour was best captured, though only by a small margin, by our capped fixed-rate model, which suggests a fixed limit in how much the implicit motor system can initially adapt. Finally, training with single-trial learning correlated and even partially predicted performance in our long fixed-rotation phase (prolonged learning), though often overestimated how much participants actually adapted in the first trial.

Discussion

While the effects of increasing perturbation size on prolonged motor adaptation have been extensively studied, its effects on early implicit adaptation are poorly understood. Our study set out to investigate this across a large range of visuomotor cursor rotations in a single-trial learning (STL) reaching paradigm. We isolated early implicit adaptation by flanking individual rotated trials between veridical feedback trials, thus allowing us to examine changes in reach aftereffects across perturbation size. Our findings show that STL is a reliable method for evoking implicit adaptation across a wide range of rotations, including rotations as small as 1º. Additionally, our capped fixed-rate model, which assumes adaptation increases up to a limit and then saturates, appeared to fit our data marginally better than our attenuation model, which assumes a decline in adaptation at larger rotations. Moreover, we explored whether predictions derived from STL could generalize to initial learning in a more traditional long-exposure paradigm and found a weak but correlated relationship between the two. Together, our findings suggest that early implicit adaptation appears to saturate rather than decline, and that STL may serve as a practical tool for predicting early-stage adaptation dynamics in longer training contexts.

Our findings indicate that single-trial learning (STL) is a reliable method for capturing implicit adaptation across a wide range of visuomotor rotations. Across all three rotation groups, significant aftereffects were observed at nearly every rotation size, with the sole exception being the 1° arc target trials. These aftereffects scaled accordingly for smaller rotations (1°–15°), averaging around 3.6°, before settling around 6° for larger rotations (15°–90°). However, what stood out to us the most was the presence of significant aftereffects with a 1° rotation in dot target trials, suggesting that the motor system can still implicitly recalibrate when faced with extremely subtle perturbations. Traditionally, studies on implicit adaptation have made use of perturbations ranging from 5° - 90°, thereby neglecting smaller perturbations that can potentially elicit implicit motor responses. That being said, a few studies have included some of these smaller perturbations while probing adaptation. For instance, Kim et al. (2018) found strong aftereffects using a 1° clamped visual perturbation, as well as with a 1.75° clamp in a subsequent study (Kim et al. 2019). STL paradigms in contrast, have yielded mixed results. Al-Fawakhiri et al. (2023) failed to find significant aftereffects when using a 1.75° clamp, while Tsay et al. (2021) found strong aftereffects, though using a 3.5° clamp. Together, our results showing the

emergence of statistically detectable aftereffects to a 1° rotation following separate single exposures, rather than multiple consecutive exposures, is to our knowledge, novel.

Our modeling results provided further insight into the underlying behaviour of initial implicit adaptation. While both our capped fixed-rate and attenuation models offered reasonable fits to our STL data, the capped fixed-rate model consistently matched the shape of our data more closely, though could not be supported statistically for how initial aftereffects scaled with rotation size. Our STL data revealed adaptation to increase with rotation size before settling around 6°, behaviour best captured by the capped fixed-rate model. In contrast, the attenuation model, which assumes a decrease in adaptation in response to larger errors, predicted a drop-off in learning at larger rotation sizes that wasn't visually apparent in our data. A paired-samples *t*-test on model MSEs supported these findings, revealing the capped fixed-rate model's predictions to be, on average, 1.73° closer to observed reaching behavior than the attenuation model. These test results were further substantiated through AICc values and relative log-likelihoods, which appeared to slightly favor the capped fixed-rate model (AIC = 54.92) over the attenuation model (AIC = 54.68).

Looking at previous works which sought to investigate how implicit adaptation scales with error, we found several studies using traditional long exposure or clamped feedback paradigms reported implicit adaptation to increase with error size up to around 20° before saturating (Bond & Taylor, 2015; Morehead et al., 2017; Kim et al., 2018; Tsay et al., 2022). However, other studies instead suggested that implicit adaptation decreased for large errors due to external error attribution, where the brain attributes large sensorimotor discrepancies to external sources and consequently devotes less resources to adapting (Wei & Körding, 2009; Tsay et al., 2021). It is also worth noting that none of the aforementioned studies probed initial implicit adaptation and instead looked at aftereffects following prolonged exposure. Thus, while the attenuation and capped fixed-rate models are based in theories that have not been previously explored in the early stages of implicit adaptation, our results, though yet to be corroborated, offered better support for the capped fixed-rate model in initial implicit adaptation.

More recently, some studies have put forth newer models that reframe the processes that drive implicit adaptation. While the mechanisms underlying implicit adaptation are not the focus of our study, the proposed models appear to correlate with that of our own. The Proprioceptive Re-Alignment Model (PReMo) put forth by Tsay et al. (2022) argues that proprioceptive errors,

discrepancies between perceived hand position and movement goals, are what truly drive implicit adaptation. Moreover, they found proprioceptive error to saturate around 5°, and like our capped-fixed rate model, the PReMo models exhibits identical behaviour, though in implicit adaptation following prolonged exposure. By contrast, the Perceptual Error Adaptation (PEA) model proposed by Zhang et al. (2024) argues that saturation in implicit adaptation is the result of uncertainty in hand position estimates, and that this uncertainty grows with visual error size. The behaviour of the PEA model assumes as a combination between our capped-fixed rate and attenuation models, where adaptation scales with small errors, peaks, then follows a concave curve as errors become larger. However, this model was also fitted to reach data following prolonged exposure, making it somewhat difficult to compare to our own data which captures initial adaptation. In sum, our data suggests that initial implicit adaptation, as captured through STL, is best characterized by a saturating response, though future research could benefit from applying these newer models to data such as our own to see whether they can better explain the earlier stages of implicit adaptation.

We also investigated if single-trial learning could anticipate early adaptation within a standard long exposure setting, and our results are encouraging. STL-based model predictions aligned well with early adaptation estimates derived from a 200-trial adaptation block using a 20° visuomotor rotation. Predictions from both the capped fixed-rate and attenuation models correlated to observed adaptation after a single rotated trial in each rotation group, with slopes spanning from 0.28 to 0.56. Although these results indicate a notable correlation, the slopes consistently fell below 1.0, implying that STL overestimated the amount of learning in the long exposure phase. We then considered whether this overestimation was actually a result of underestimation from our exponential decay function used to estimate initial adaptation. However, further analyses comparing exponential fits to observed reaches on the first rotated trial revealed no significant differences, indicating that our exponential function did not systematically misestimate early adaptation and, if anything, slightly overpredicted it.

To the best of our knowledge, no existing research has directly attempted to predict long exposure adaptation using single-trial learning. While prior studies such as that by Ruttle et al. (2016, 2021) and D'Amario et al. (2024) measured reach aftereffects following one or a few rotated trials, they did not generate model-based predictions from STL, and instead modelled implicit adaptation through exponential decay. As such, our findings may represent a novel

contribution to the field. Moreover, these results present a new possible direction of research in how well STL can map adaptation across a broader range of perturbation sizes and learning contexts. We are still unsure whether the overestimations we observed were due to use of the 20° rotation in the long exposure phase, and whether the same trend would present if we were to test smaller or larger perturbations. When looking at the time course of implicit adaptation, D'Amario et al. (2024) tested four separate rotation groups (15°, 30°, 45°, and 60°). Future studies could benefit from testing a broader range of rotations in long exposure contexts akin to that of D'Amario et al. (2024), and then comparing them to STL predictions. Doing so could potentially provide a clearer idea as to whether the overestimations we observed in our experiment are consistent or varied across error size. It may also be informative to interleave no-cursor trials throughout longer adaptation blocks in future work to track implicit changes more continuously and assess how well STL generalizes to these long exposure contexts.

Conclusion

To conclude, the results of our exploratory study support the idea that initial implicit adaptation emerges rapidly, increases with error size up to a fixed limit, and can be reliably captured using a single-trial learning (STL) approach. Moreover, our STL results revealed significant aftereffects in visuomotor rotations as small as 1°, highlighting the sensitivity of the implicit motor system in responding to very small errors immediately following exposure. The saturation effect in adaptation that we observed at larger rotation sizes falls in line with the possibility of a capped internal correction mechanism in the early stages of adaptation, rather than being attenuated by external error attribution. Furthermore, the modest, yet consistent ability of our STL-based models in predicting early adaptation behaviour in a prolonged exposure condition points to the possibility of STL paradigms offering a practical and more efficient means of probing performance outcomes in prolonged learning contexts. While our findings have yet to be corroborated in future studies, they not only refine our understanding of the dynamics of early motor learning but also give credence to STL as a valuable approach for investigating the constraints and continuity of implicit processes across different adaptation contexts.

References

Al-Fawakhiri, N., Ma, A., Taylor, J. A., & Kim, O. A. (2023). Exploring the role of task success in implicit motor adaptation. *Journal of Neurophysiology*, *130*(2), 332–344. https://doi.org/10.1152/jn.00061.2023

Bastian A. J. (2008). Understanding sensorimotor adaptation and learning for rehabilitation. *Current opinion in neurology*, *21*(6), 628–633. https://doi.org/10.1097/WCO.0b013e328315a293

Bond, K. M., & Taylor, J. A. (2015). Flexible explicit but rigid implicit learning in a visuomotor adaptation task. *Journal of Neurophysiology*, *113*(10), 3836–3849. https://doi.org/10.1152/jn.00009.2015

D'Amario, S., Ruttle, J. E., 't Hart, B. M., & Henriques, D. Y. (2024). Implicit Adaptation is Fast, Robust and Independent from Explicit Adaptation. *bioRxiv*, 2024-04.

Gastrock, R. Q., Modchalingam, S., 't Hart, B. M., & Henriques, D. Y. (2020). External error attribution dampens efferent-based predictions but not proprioceptive changes in hand localization. *Scientific Reports*, *10*(1). https://doi.org/10.1038/s41598-020-76940-3

Hayashi, T., Kato, Y., & Nozaki, D. (2020). Divisively normalized integration of multisensory error information develops motor memories specific to vision and proprioception. *The Journal of Neuroscience*, *40*(7), 1560–1570. https://doi.org/10.1523/jneurosci.1745-19.2019

Kim, H. E., Morehead, J. R., Parvin, D. E., Moazzezi, R., & Ivry, R. B. (2018). Invariant errors reveal limitations in motor correction rather than constraints on error sensitivity. *Communications Biology*, *1*(1). https://doi.org/10.1038/s42003-018-0021-y

Kim, H. E., Parvin, D. E., & Ivry, R. B. (2019). The influence of task outcome on implicit motor learning. eLife, 8, e39882. https://doi.org/10.7554/eLife.39882

Kim, O. A., Forrence, A. D., & McDougle, S. D. (2022). Motor learning without movement. *Proceedings of the National Academy of Sciences*, *119*(30). https://doi.org/10.1073/pnas.2204379119

Körding KP, Beierholm U, Ma WJ, Quartz S, Tenenbaum JB, et al. (2007) Causal Inference in Multisensory Perception. *PLoS ONE* 2(9): e943. https://doi.org/10.1371/journal.pone.0000943

Krakauer, J. W., Hadjiosif, A. M., Xu, J., Wong, A. L., & Haith, A. M. (2019). Motor learning. *Comprehensive Physiology*, 613–663. https://doi.org/10.1002/cphy.c170043

Marko, M. K., Haith, A. M., Harran, M. D., & Shadmehr, R. (2012). Sensitivity to prediction error in reach adaptation. *Journal of Neurophysiology*, *108*(6), 1752–1763. https://doi.org/10.1152/jn.00177.2012

Mazzoni, P., & Krakauer, J. W. (2006). An implicit plan overrides an explicit strategy during visuomotor adaptation. *The Journal of Neuroscience*, *26*(14), 3642–3645. https://doi.org/10.1523/jneurosci.5317-05.2006

Miall, R. C., & Wolpert, D. M. (1996). Forward models for Physiological Motor Control. *Neural Networks*, *9*(8), 1265–1279. https://doi.org/10.1016/s0893-6080(96)00035-4

Modchalingam, S., Ciccone, M., D'Amario, S., 't Hart, B. M., & Henriques, D. Y. P. (2023). Adapting to visuomotor rotations in stepped increments increases implicit motor learning. *Scientific reports*, *13*(1), 5022. https://doi.org/10.1038/s41598-023-32068-8

Modchalingam, S., Vachon, C. M., ’t Hart, B. M. & Henriques, D. Y. P. (2019). The effects of awareness of the perturbation during motor adaptation on hand localization. *PLoS ONE* 14, 1–20. https://doi.org/10.1371/journal.pone.0220884

Morehead, J. R., Taylor, J. A., Parvin, D. E., & Ivry, R. B. (2017). Characteristics of implicit sensorimotor adaptation revealed by task-irrelevant clamped feedback. *Journal of Cognitive Neuroscience*, *29*(6), 1061–1074. https://doi.org/10.1162/jocn_a_01108

Neville, K.-M., & Cressman, E. K. (2018). The influence of awareness on explicit and implicit contributions to visuomotor adaptation over time. *Experimental Brain Research*, *236*(7), 2047–2059. https://doi.org/10.1007/s00221-018-5282-7

Ruttle JE, Cressman EK, 't Hart BM, Henriques DYP (2016) Time Course of Reach Adaptation and Proprioceptive Recalibration during Visuomotor Learning. *PLoS ONE* 11(10): e0163695. https://doi.org/10.1371/journal.pone.0163695

Ruttle, J. E., 't Hart, B. M., & Henriques, D. Y. (2021). Implicit motor learning within three trials. *Scientific Reports*, *11*(1). https://doi.org/10.1038/s41598-021-81031-y

Taylor JA, Ivry RB (2011) Flexible Cognitive Strategies during Motor Learning. PLOS Computational Biology 7(3): e1001096. https://doi.org/10.1371/journal.pcbi.1001096

Taylor, J. A., & Ivry, R. B. (2012). The role of strategies in motor learning. Annals of the New York Academy of Sciences, 1251, 1–12. https://doi.org/10.1111/j.1749-6632.2011.06430.x

Tsay, J. S., Avraham, G., Kim, H. E., Parvin, D. E., Wang, Z., & Ivry, R. B. (2021). The effect of visual uncertainty on implicit motor adaptation. *Journal of Neurophysiology*, *125*(1), 12–22. https://doi.org/10.1152/jn.00493.2020

Tsay, J. S., Kim, H., Haith, A. M., & Ivry, R. B. (2022). Understanding implicit sensorimotor adaptation as a process of proprioceptive re-alignment. *eLife*, *11*. https://doi.org/10.7554/elife.76639 y

Vandevoorde, K., & Orban de Xivry, J.-J. (2019). Internal model recalibration does not deteriorate with age while motor adaptation does. *Neurobiology of Aging*, *80*, 138–153. https://doi.org/10.1016/j.neurobiolaging.2019.03.020

Wei, K., & Körding, K. (2009). Relevance of error: What drives motor adaptation? *Journal of Neurophysiology*, *101*(2), 655–664. https://doi.org/10.1152/jn.90545.2008

Zhang, Z., Wang, H., Zhang, T., Nie, Z., & Wei, K. (2024). *Perceptual Error Based on Bayesian Cue Combination Drives Implicit Motor Adaptation*. https://doi.org/10.7554/elife.94608.1